Title

Immune Modulation with RANKL Blockade through Denosumab Treatment in Patients with Cancer.

Journal

Cancer Immunology Research, 12(4)

Authors

Chang, Hewitt
Marquez, Jaqueline
Chen, Brandon
et al.

Publication Date

2024-04-02

DOI

10.1158/2326-6066.CIR-23-0184

Peer reviewed

Immune Modulation with RANKL Blockade through Denosumab Treatment in Patients with Cancer

Hewitt Chang[1], Jaqueline Marquez[1], Brandon K. Chen[1], Daniel M. Kim[1], Michael L. Cheng[1], Eric V. Liu[1], Hai Yang[2], Li Zhang[1,2], Meenal Sinha[1], Alexander Cheung[1], Serena S. Kwek[1], Eric D. Chow[1,3], Mark Bridge[4], Rahul R. Aggarwal[1,4], Terence W. Friedlander[1], Eric J. Small[1,4], Mark Anderson[5], and Lawrence Fong[1,4]

ABSTRACT

Denosumab is a fully human mAb that binds receptor activator of NFκB ligand (RANKL). It is routinely administered to patients with cancer to reduce the incidence of new bone metastasis. RANK–RANKL interactions regulate bone turnover by controlling osteoclast recruitment, development, and activity. However, these interactions also can regulate immune cells including dendritic cells and medullary thymic epithelial cells. Inhibition of the latter results in reduced thymic negative selection of T cells and could enhance the generation of tumor-specific T cells. We examined whether administering denosumab could modify modulate circulating immune cells in patients with cancer. Blood was collected from 23 patients with prostate cancer and 3 patients with renal cell carcinoma, all of whom had advanced disease and were receiving denosumab, prior to and during denosumab treatment. Using high-dimensional mass cytometry, we found that denosumab treatment by itself induced modest effects on circulating immune cell frequency and activation. We also found minimal changes in the circulating T-cell repertoire and the frequency of new thymic emigrants with denosumab treatment. However, when we stratified patients by whether they were receiving chemotherapy and/or steroids, patients receiving these concomitant treatments showed significantly greater immune modulation, including an increase in the frequency of natural killer cells early and classical monocytes later. We also saw broad induction of CTLA-4 and TIM3 expression in circulating lymphocytes and some monocyte populations. These findings suggest that denosumab treatment by itself has modest immunomodulatory effects, but when combined with conventional cancer treatments, can lead to the induction of immunologic checkpoints.

See related Spotlight by Nasrollahi and Davar, p. 383.

Introduction

Denosumab is FDA approved for the prevention of skeletal-related events (SRE) in patients with bone metastases from solid malignancies as well as in patients with nonmetastatic prostate cancer who are receiving androgen deprivation therapy and patients with breast cancer who are receiving adjuvant aromatase inhibitor therapy. Osteoblasts and osteoclasts, respectively responsible for bone formation and bone resorption, are critical in maintaining the skeletal structure. To maintain a balance between bone formation and resorption, osteoblasts express receptor activator of NFκB ligand (RANKL) and osteoclast precursors express RANK receptor. This RANK–RANKL system drives osteoclast stimulation and function. The RANK–RANKL interaction can be inhibited by the endogenous decoy receptor osteoprotegerin (1) or therapeutically by denosumab. Denosumab is a fully human mAb that interferes with RANK–RANKL interactions and inhibits osteoclast maturation, recruitment, and activity (2).

The RANK–RANKL pathway also plays critical roles in the development and regulation of the immune system, especially with regard to the regulation of dendritic cell (DC) activity. RANKL is primarily expressed on $CD4^+$ and $CD8^+$ T cells following stimulation and interfaces with RANK, which is highly expressed on DCs. RANKL has been shown to enhance DC survival (3), potentially via induction of the antiapoptotic protein B-cell lymphoma-extra large (Bcl-xL; ref. 4) and the antiapoptotic serine/threonine kinase AKT/PKB (5). RANKL also induces DC expression of multiple activating cytokines, including IL1, IL6, IL12, and IL15. While RANKL–RANK signaling has been shown to be important in immune activation, this interaction may also have a role in immunosuppression: RANKL has been shown to induce T-cell tolerance via expansion of $CD4^+CD25^+$ regulatory T cells (Treg; ref. 6). RANK–RANKL signaling also plays a key biological role in immune system development. RANKL is required for proper lymph node development and the RANK–RANKL pathway regulates proliferation of medullary thymic epithelial cells (mTEC) and thymic medulla formation, which ultimately contribute to establishment of self-tolerance (7).

Preclinical observations have revealed that the RANK–RANKL axis is involved in the modulation of DCs and the negative selection of developing thymic produced naïve T cells (3–7). The effects of denosumab on immune activation are not well understood, leading to uncertainty as to whether this drug might enhance or inhibit immunotherapies including immune checkpoint inhibitors. Therefore, we initiated a prospective, nonrandomized, biobanking protocol with patients that presented with bone metastases, solid malignancies—other than multiple myeloma—and received standard-of-care denosumab treatment.

[1]Division of Hematology/Oncology, Department of Medicine, University of California San Francisco, San Francisco, California. [2]Department of Epidemiology and Biostatistics, University of California San Francisco, San Francisco, California. [3]Department of Biochemistry and Biophysics, Center for Advanced Technologies, University of California San Francisco, San Francisco, California. [4]Helen Diller Family Comprehensive Cancer Center, University of California San Francisco, San Francisco, California. [5]Diabetes Center, Department of Medicine, University of California San Francisco, San Francisco, California.

Corresponding Author: Lawrence Fong, Fred Hutchinson Cancer Center, 1100 Fairview Ave N, Seattle, WA 98109. E-mail: lawrence.fong@fredhutch.org

Cancer Immunol Res 2024;12:453–61

doi: 10.1158/2326-6066.CIR-23-0184

Materials and Methods

Study design

This study was a prospective, nonrandomized, biobanking protocol at University of California, San Francisco (UCSF) to obtain serial blood samples from patients starting standard-of-care denosumab (120 mg every 4 weeks). All patients or their legally accepted representatives provided written informed consent to participate after being informed of the nature, purpose, participation conditions, and standard risks of phlebotomy. Key eligibility criteria for this study included patients had to be ages 18 or older with a histologically confirmed diagnosis of solid tumor malignancy (other than multiple myeloma) with bone metastasis and qualify to receive treatment with denosumab for prevention of SREs. Patients who received new systemic treatment (either intravenous or oral) within 4 weeks of the start of denosumab initiation were excluded from the study.

Patients had blood drawn for peripheral blood mononuclear cell (PBMC) isolation and cryopreservation at the following time points: screening visit (pre-denosumab, TP1), prior to second denosumab injection (TP2), prior to third denosumab injection (TP3), prior to sixth denosumab injection (TP4). To assess any potential interactions with immunotherapies, additional blood could be drawn pretreatment and posttreatment when a patient was transitioning to an immune-based therapy, including sipuleucel-T and ipilimumab.

A total of 26 patients with advanced disease enrolled on this protocol, 23 patients with prostate cancer and 3 patients with renal cell carcinoma. Characteristics of trial participants are summarized in Supplementary Table S1. This collection was approved by the UCSF Institutional Review Board and conducted as a single institution trial (protocol CC#13982). This study was conducted in accordance with Declaration of Helsinki, Belmont Report, Nuremberg Code, and National Bioethics Advisory Commission.

High-dimensional cytometry by time of flight (CyTOF) Banked cryopreserved PBMCs from the study were thawed, barcoded, and stained with metal-labeled antibodies to create an immune-monitoring panel for PBMCs and T-cell subsets (for details of the antibodies, see Supplementary Table S2). Mass tag barcoding of samples was performed by incubating cells with distinct combinations of isotopically-purified palladium ions chelated by isothiocyanobenzyl-EDTA (Fluidigm, catalog no. 201060). Samples were washed and data collected through mass cytometry (Helios, Fluidigm). Data were then prepared for analysis using the R Premessa 0.2.0 package (https://github.com/ParkerICI/premessa/). Barcodes were run through CytoNorm (ref. 8; https://github.com/saeyslab/CytoNorm) to correct for small batch variances using several samples that were run redundantly to serve as validation samples between different barcodes, clustering samples to normalize the data between files. PBMCs were extracted from FCS files and divided into 200 unsupervised clusters using statistical scaffold analysis and clusters were entered into a force-directed graph centered around predetermined landmark nodes made by manual gating on Cytobank (9) as shown in the supplementary gating strategy (Supplementary Fig. S1). Calculations for clustering [by both Uniform Manifold Approximation and Projection (UMAP) and Scaffold] were performed based upon the relative staining of CD3, CD4, CD8a, CD11b, CD11c, CD14, CD19, CD25, CD31, CD33, CD45RA, CD15, CD123, TCRgd, CD56, Tbet, FceR1a, CCR7, FoxP3, HLA-DR, CD61_CD235ab, CD19, CD45, and CD16. Cluster frequency and Boolean expressions for markers in each cluster were passed through Significance Across Microarrays algorithm and the results were formulated into Scaffold maps for visualization (https://github.com/spitzerlab/statisticalscaffold). Scaffold heat maps, fold changes, significances, cell counts, and nearest landmark nodes were extracted and visualized using custom script to generate heat maps using R pheatmap package (https://CRAN.R-project.org/package=pheatmap). UMAP was downsampled to 1,000 cells from each of the 74 samples and generated by using the uwot package (https://github.com/jlmelville/uwot) for dimensionality reduction and Rphenograph (ref. 10; https://github.com/JinmiaoChenLab/Rphenograph) for clustering.

T-cell receptor sequencing

Cryopreserved PBMCs were thawed and 250,000 cells were extracted for RNA using the Invitrogen RNAqueous-Micro Total RNA Isolation Kit (Thermo Fisher Scientific #AM1931). A total of 10.4 ng of RNA was used for reverse transcription (RT) and cDNA generation, following the Smart-seq2 protocol with modifications as described here (11). The oligo-dT primer was biotinylated at the 5′ end. We added a barcode, unique molecular modifiers, and biotin to the 5′ end of the TSO primer (Integrated DNA Technologies, Primer sequences in Supplementary Table S3). Maxima H Minus Reverse Transcriptase (Thermo Fisher Scientific #EP0753) was used for RT. Barcoded RT product was then pooled together and purified using a DNA Clean & Concentrator-5 Kit (Zymo Research, #D4013). A total of 16 cycles were used for cDNA amplification. cDNA was then enriched for alpha and beta T-cell receptors (TCR) separately and used for Illumina library generation by PCR (Integrated DNA Technologies, Primer sequences in Supplementary Table S3). Libraries were sequenced on a NovaSeq 6000 and run across two SP 300 lanes with run parameters 22×6×0×297 (R1×I1×I2×R2).

TCR sequencing analysis

Sample barcodes were used to separate each sample from the library pool and the data were preprocessed with MiXCR version 3.0.13. Among 81 samples with valid TCR sequencing, we had 69 evaluable samples. Clonality (12) and TCR convergent frequency (13) were used to measure the global TCR metrics. TCR relative clonality (RCL, i.e., ratio of clonality at later time point vs. baseline clonality) and TCR clonality were used to measure the treatment effect. The comparison between posttreatment time points and baseline was done by Wilcoxon signed-rank test. The comparison between the two groups was done by the Wilcoxon rank-sum test. No adjustments for multiple testing were done.

TCR excision circle and RANKL quantitation

Cryopreserved PBMCs were thawed and 300,000 to 400,000 cells per patient time point were extracted for DNA using a QIAamp DNA Blood Mini Kit (Qiagen, #51104) following the manufacturer's protocol. A total of 10–100 ng of DNA was used for quantification of T-cell receptor excision circles (TREC) by RT-PCR with a TRECSProbe (Applied Biosystems #45002), Actin Probe (5′- 6FAM ATG CCC TCC CCC ATG CCA TCC TGC GT TAMRA - 3′), and TaqMan (Applied Biosystems #4326708). Plates were prepared per Applied Biosystems recommendations for the StepOnePlus Real-Time PCR System (Thermo Fisher Scientific #4376598) and amplified for 40 total cycles. Standard curves of tRNA were prepared on every reaction plate in triplicate for a detectable range for 100,000 to 12 TREC copies and β-actin (Supplementary Fig. S2A).

The RANKL qPCR was carried out with *RANKL* TaqMan Gene Expression Assay (FAM, Hs00243522_m1 catalog no. 4331182) and internal control actin-B, ACTB TaqMan Gene Expression Assay (VIC,

Hs01060665_g1 catalog no. 4448489, diluted 1:8 in dH2O) using TaqMan Gene Expression Master Mix Kit Life Technologies (catalog no. 4369016) on cDNA generated with High-Capacity RNA-to-cDNA Kit Life Technologies (catalog no. 4387406), from 5 ng of RNA extracted from 250,000 PBMC. Delta C_t (cycle threshold) is C_t of RANKL minus C_t of ACTB in each sample. Fold change is $2^{-\text{delta delta Ct}}$. Delta delta C_t is delta C_t of time point 2 or time point 3 minus delta C_t of pretreatment time point 1.

RANKL ELISA

Human TNFSF11 (RANKL) ELISA Kit was used to quantitate soluble RANKL protein in human plasma (Abcam, ab213841). Previously frozen plasma from patients' samples were thawed at room temperature, spun at 1,500 × *g* for 15 minutes and 100 μL of supernatant was loaded into duplicate wells of the ELISA plate. RANKL was quantitated according to the manufacturer's instructions.

Statistical analysis

In general, continuous outcomes were summarized by median and interquartile range, compared between time points by Wilcoxon signed-rank test, and compared between groups by Wilcoxon rank-sum test. Statistical significance was declaimed on the basis of P value < 0.05 unless otherwise noted. Major statistical analysis was done by using the statistical computing software R unless noted.

Data availability

Mass cytometry data will be shared publicly on FlowRepository while R-based analysis codes are available at https://github.com/fonglab/scaffold-heatmap-pub. The TCR sequencing data generated in this publication have been deposited in NCBI's Gene Expression Omnibus (GEO) and are accessible through GEO Series accession number GSE248774. All other data generated in this study are available within the article and its Supplementary Data or upon request from the corresponding author.

Ethics approval and consent to participate

Relevant Institutional Review Boards at UCSF approved the study protocol (CC#13982), which allowed for patient biospecimen collection on patients receiving standard-of-care denosumab for metastatic cancer. Each patient provided signed informed consent prior to enrollment.

Consent for publication

All authors have provided their consent to the publication of this work.

Results

We obtained written informed consent and collected PBMC samples from patients with cancer with bone metastasis receiving standard-of-care denosumab treatment (**Fig. 1A**). High-dimensional CyTOF was used to assess the effects of denosumab in the circulating immune compartment (**Fig. 1B**). Because RANKL is expressed on myeloid cells, we initially assessed for changes in the different myeloid-cell populations between the pretreatment baseline time point (TP1) and the on-treatment time point 3 (TP3). We did not see any significant changes in frequencies of myeloid cells (no blue or red nodes on scaffold map) of the different myeloid-cell populations (**Fig. 1C**). Heat maps were then used to assess for changes in phenotypic marker expression across the myeloid-cell populations. Although there were minimal changes on circulating myeloid cells overall, we did observe a transient increase in CD137 expression on some populations of conventional DCs, classical monocytes, and intermediate monocytes in TP2, but these were lost in subsequent time points. We also observed transient increases in PD-L1 and TIM3 expression on the classical and intermediate monocyte cell populations at TP3 (**Fig. 1D**).

Next, we interrogated the lymphocyte compartment to assess whether RANKL inhibition can lead to downstream effects on effector populations. We again did not observe a statistically significant difference in the frequency of various lymphocyte populations after denosumab treatment (**Fig. 2A**). Similar to the myeloid-cell populations, we observed modest changes in activation markers overall and a transient increase in CD137 on naïve $CD4^+$ T cells, and Tregs, and a rare population of natural killer T (NKT) cells at TP2. We also observed transient increases in PD-L1 on naïve $CD8^+$ T cells and NKT cells. We saw transient increases at TP3 in CD40 on naïve and effector $CD4^+$ T cells, and Ki-67 on effector $CD8^+$ T cells (**Fig. 2B**). With additional doses of denosumab at TP4, we no longer observed these changes. We also observed expression of the immune checkpoint markers PD-L1, TIM3, and CTLA-4, irrespective of denosumab and concomitant therapies, prior to denosumab treatment at TP1 and posttreatment (Supplementary Fig. S3A and S3B). Thus, changes observed in our time point comparisons of functional markers are relative to a baseline level of expression.

To examine whether *RANKL* expression was affected in circulating immune cells, we quantified mRNA expression pretreatment and posttreatment. Relative to pretreatment expression levels of *RANKL*, changes in *RANKL* expression were minimal. However, we observed a trend toward a decrease in the expression of *RANKL* in circulating immune cells at TP3 (Supplementary Fig. S2B; $P = 0.055$). We next quantified the amount of circulating RANKL from plasma samples at TP1 and TP3. In contrast with the trend of decreased RANKL expression, overall, the amount of soluble RANKL was low and we did not observe statistically significant changes after denosumab treatment (Supplementary Fig. S2C).

Next, we interrogated whether RANKL inhibition could effect changes in the T-cell repertoire. We performed TCR β chain sequencing on serial PBMCs (**Fig. 3A**). We found that clonality at TP3—after the two treatments of denosumab—trended higher compared with the clonality at baseline and after the first injection of denosumab (**Fig. 3B**). We also examined TCR convergent frequency across the course of treatment but only saw modest changes in convergence between time points (**Fig. 3C**).

We examined whether denosumab could alter the frequency of recent thymic emigrants. We quantified TRECs across patient treatment time points. The level of TRECs was similar across the time points and there was no statistically significant change after denosumab treatment (**Fig. 4A**). Because these patients were receiving denosumab for metastatic cancer as standard of care, some of the patients concurrently received chemotherapy, steroids, or both, as part of their treatment. Although not statistically significant, we observed that treatment with chemotherapy, steroids, or both, reduced the amount of TRECs (**Fig. 4B**). Furthermore, there was no difference in *RANKL* mRNA expression between the two groups (Supplementary Fig. S2D).

To determine whether there were any broad effects of chemotherapy or steroids, or both, during the course of denosumab treatment, we performed statistical scaffold analysis comparing TP1 with on-treatment time points separating the patients by whether or not they were receiving these other treatments. The patients who received concurrent chemotherapy or steroids, or both, showed broad changes

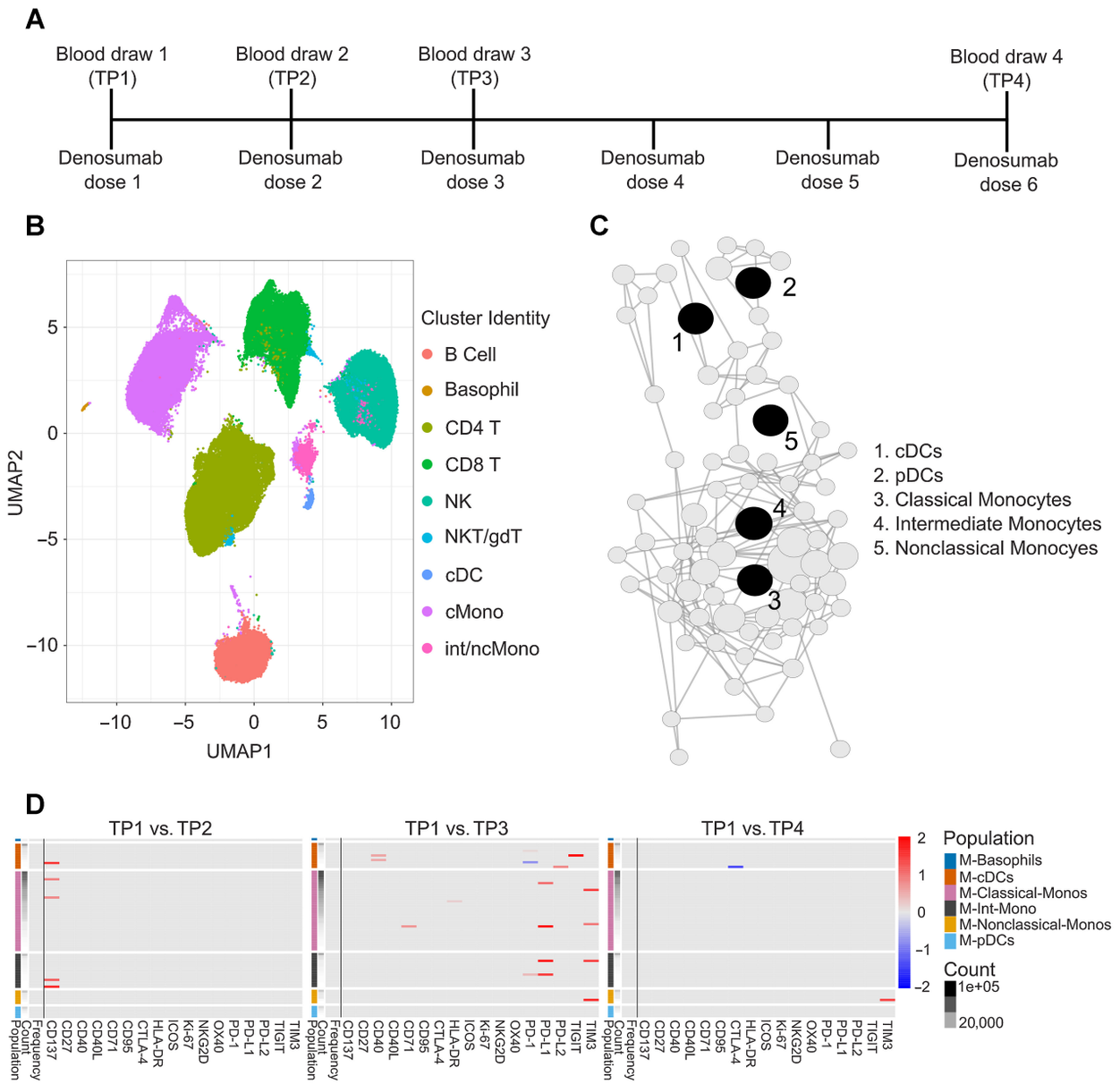

Figure 1.

Modulation of circulating myeloid cells with denosumab treatment. **A,** Schema outlining when patients received denosumab treatment and when blood samples were drawn. Blood samples were drawn prior to denosumab treatment. **B,** A UMAP plot of cells from all PBMC samples analyzed with Scaffold using data from CyTOF. Clusters correspond to canonical immune cells and are represented by distinct colors. **C,** Scaffold maps of the frequency of myeloid cell clusters are shown comparing pretreatment time point (TP) 1 ($n = 16$) with TP3 ($n = 14$). Black nodes represent landmark nodes of myeloid cell types identified by traditional manual cell gating. Remaining nodes represent unsupervised myeloid cell clusters created by scaffold analysis. Nodes are arranged and connected around each other, and the distance between connected nodes depends on cluster similarity. Cluster size is proportional to cellular abundance. The color of the nodes indicates statistically significant differences ($q < 0.05$; red = increase, blue = decrease, gray = not significant) between the two time points. There are no nodes with blue or red indicating that there are no myeloid populations that are significantly changed in frequency with treatment. **D,** Heat maps summarizing $\log_2$ fold changes from statistical analysis of functional markers CD137, CD27, CD40, CD40L, CD71, CD95, CTLA-4, HLA-DR, ICOS, Ki-67, NKG2D, OX40, PD-1, PD-L1, PD-L2, TIGIT, and TIM3 when comparing pretreatment time point TP1 ($n = 16$) with TP3 ($n = 14$) and TP4 ($n = 7$). Each box in the heat map represents a myeloid cell cluster that was labeled according to the nearest landmark node they connect to on the scaffold map and ordered by cell count abundance. The pseudocolor represents clusters that showed a significant difference ($q < 0.05$) in the $\log_2$ fold change, with red being significantly higher, while blue being significantly lower in group 2 of the two comparison groups.

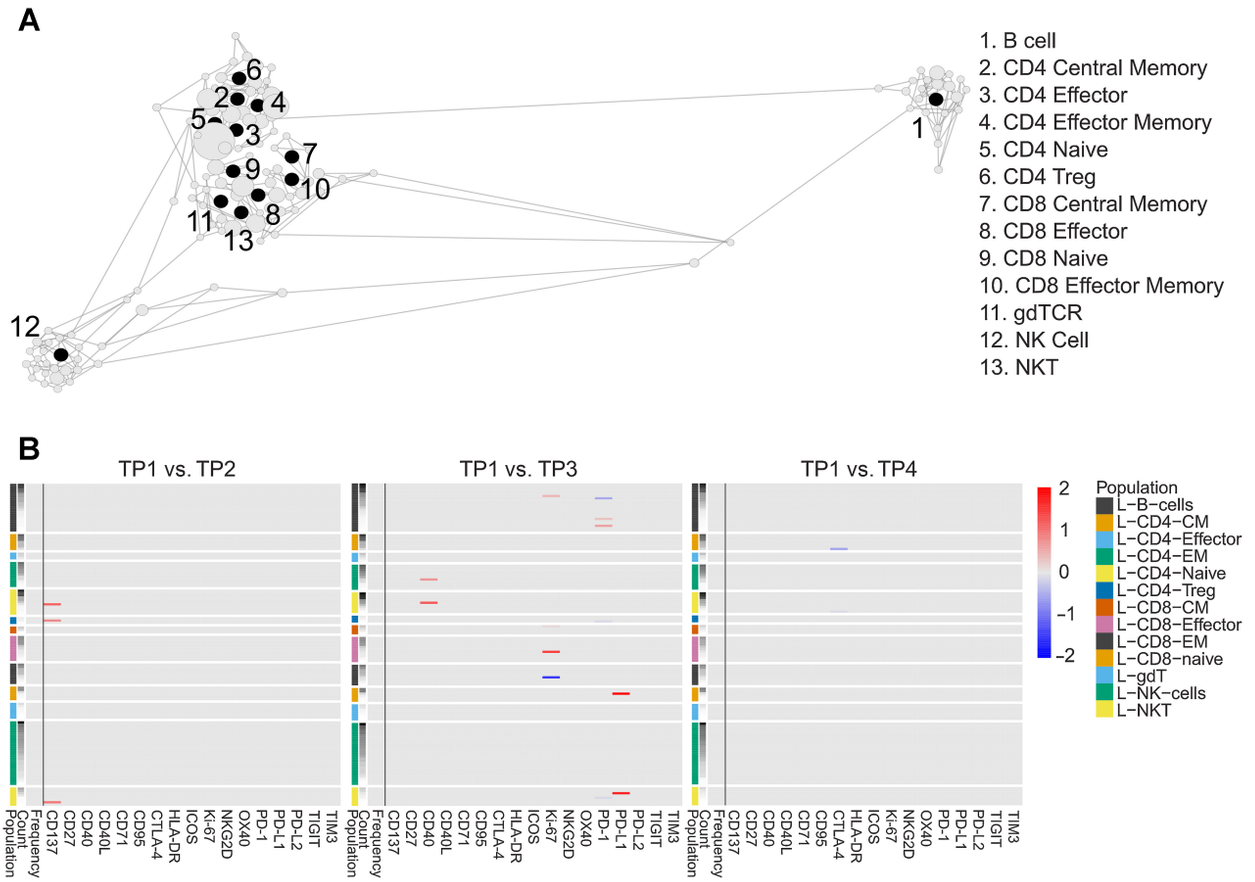

Figure 2.

Modulation of circulating immune effectors with denosumab treatment. **A,** Scaffold map of significant changes in the frequency of lymphocyte cell subsets. Clusters are shown comparing pretreatment TP1 ($n = 16$) with TP4 ($n = 7$). Scaffold was used to analyze PBMC data obtained from CyTOF. **B,** Heat maps summarizing $\log_2$ fold changes from statistical analysis of functional markers CD137, CD27, CD40, CD40L, CD71, CD95, CTLA-4, HLA-DR, ICOS, Ki-67, NKG2D, OX40, PD-1, PD-L1, PD-L2, TIGIT, and TIM3 when comparing pretreatment time point TP1 ($n = 16$) with TP3 ($n = 14$) and TP4 ($n = 7$). Each box in the heat map represents a lymphocyte cluster that was labeled according to the nearest landmark node they connect to on the scaffold map and ordered by cell count abundance. The pseudocolor represents clusters that showed a significant difference ($q < 0.05$) in the $\log_2$ fold change, with red being significantly higher, while blue being significantly lower in group 2 of the two comparison groups.

with denosumab treatment whereas patients who received denosumab without these concomitant treatments did not (**Fig. 5A**). In patients receiving these concomitant treatments, the changes with treatment included significantly higher levels of CTLA-4 and TIM3 after treatment across a broad range of lymphoid- and myeloid-cell populations. When comparing these patient groups at pretreatment TP1, patients who received chemotherapy, steroids, or both, before denosumab showed greater immune modulation across the myeloid- and lymphoid-cell populations (Supplementary Fig. S4). When we removed patients who received steroids and compared patients who only received chemotherapy with patients who did not receive concurrent treatment prior to denosumab, we observed similar changes (Supplementary Fig. S5A). We further separated the concurrent treatments patients received into three groups and compared them at TP2 and TP3: patients who received chemotherapy or chemotherapy and steroids, patients who received only steroids, and patients who did not receive chemotherapy or steroids. Similar to our comparison of concomitant treatments, we observed broad changes in activation markers between the groups and modest differences in the frequency of immune cell populations in the lymphoid- and myeloid-cell compartments (Supplementary Fig. S5A–S5C). We also evaluated the effects of chemotherapy and steroids on the T-cell repertoire. To interrogate changes in the TCR sequences, we compared the clonality between the patients who only received denosumab and those who also received denosumab with concomitant chemotherapy, steroids, or both at all time points (**Fig. 5B**). We found a trend toward increased TCR clonality in patients who received concomitant therapies across all time points. We also found that the relative clonality from baseline to TP3 was higher in the patients who received chemotherapy, steroids, or both, though it was not statistically significant (**Fig. 5C**; 1.17 vs. 1.04, $P = 0.073$).

Discussion

Denosumab is used to prevent SREs and bone metastasis in multiple cancer types. However, the RANK–RANKL axis has been shown to play a role in inducing DC expression of stimulatory cytokines (14) and in regulating the homeostasis of Tregs (15). Because of the effects of the RANK–RANKL axis on the immune system, patients receiving denosumab have been excluded from many immunotherapy trials.

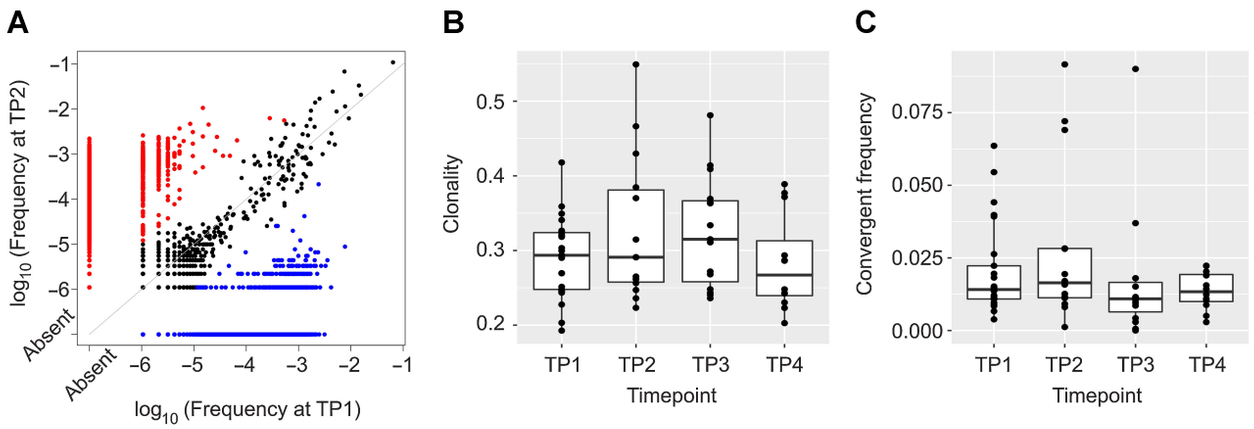

Figure 3.

Changes in the peripheral T-cell repertoire with denosumab treatment. **A,** TCR β chain sequencing was performed on longitudinal samples from patients. Clonotypic frequencies of a representative patient are shown with pretreatment time point (TP1) on the horizontal axis and posttreatment time point (TP2) on the vertical axis. Clonality (**B**) and TCR convergent frequency (**C**) were calculated and compared across the time points using the Wilcoxon signed-rank test [TP1 ($n = 25$), TP2 ($n = 14$), TP3 ($n = 15$), TP4 ($n = 12$)]. In these box and whisker plots, the box covers the interquartile range, the horizontal line that splits the box is the median, and the whiskers capture the minimum and maximum.

However, RANK–RANKL interactions are also critical for the development of mTECs, which express autoimmune regulator (Aire) and are critical in mediating the negative selection of autoreactive T cells (7). Indeed, preclinical models have shown that RANKL blockade can enhance antitumor immune responses as well as enhance the efficacy of immune checkpoint inhibition (16–19). One study in a murine model found that treatment with RANKL blockade increases the frequency of $CD4^+$ single positive T cells (17). While another showed that RANKL and CTLA-4 blockade in combination increases the frequency of tumor-infiltrating lymphocytes (20). An additional study reported increased $CD8^+$ T-cell frequency in blood and tissue of murine models and in paired blood and tumor tissue from patients with breast cancer after denosumab treatment (21). In contrast, our study focused on interrogating the circulating immune cells of patients with metastatic cancer receiving denosumab through longitudinal sampling of PBMCs. Our data comparing PBMC samples at pretreatment with posttreatment time points demonstrated no significant changes in circulating immune cell frequencies. We found only modest changes in the phenotype of circulating myeloid- and lymphoid-cell populations. Additional studies should be conducted to validate the effects of denosumab on immune cell frequencies.

Because of preclinical models showing modulation of T cells, we further interrogated how denosumab affected the T-cell repertoire by

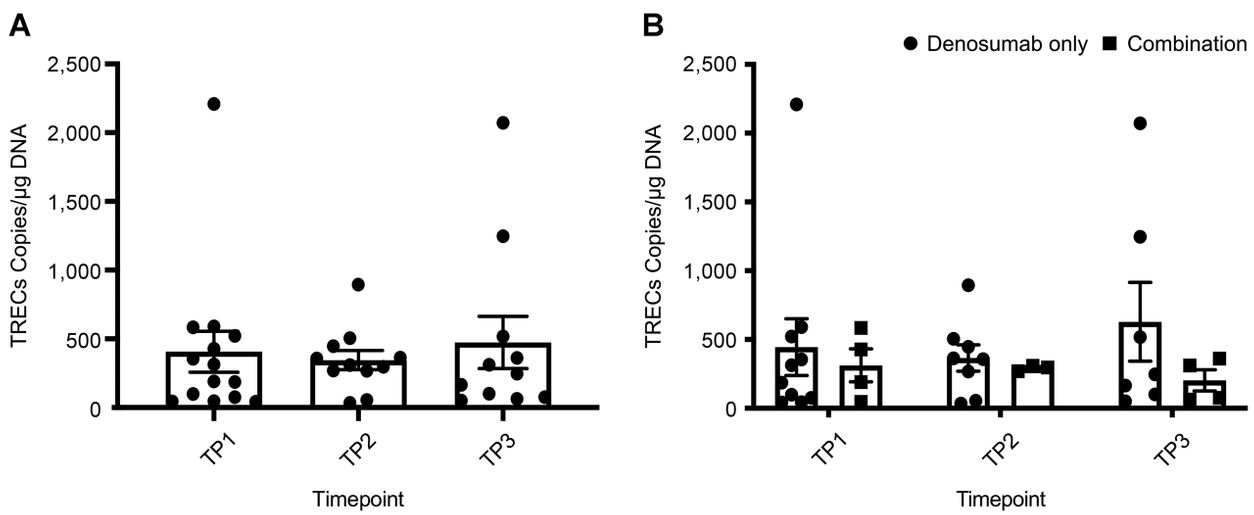

Figure 4.

Effects of treatment on recent thymic emigrants. DNA isolated from PBMCs was assessed by qPCR for changes in copies of TRECs. **A,** Comparisons of TREC copies were done across time points for all patients ($n = 14$). Statistical analyses were calculated using the Wilcoxon signed-rank test (mean ± SEM). **B,** TREC copies were compared between patients who received chemotherapy, steroids, or both (combination, $n = 4$) to patients who did not receive chemotherapy or steroids (denosumab only, $n = 10$). Statistical analyses were calculated using the Wilcoxon signed-rank test between time points and the Wilcoxon rank-sum test between groups (mean ± SEM).

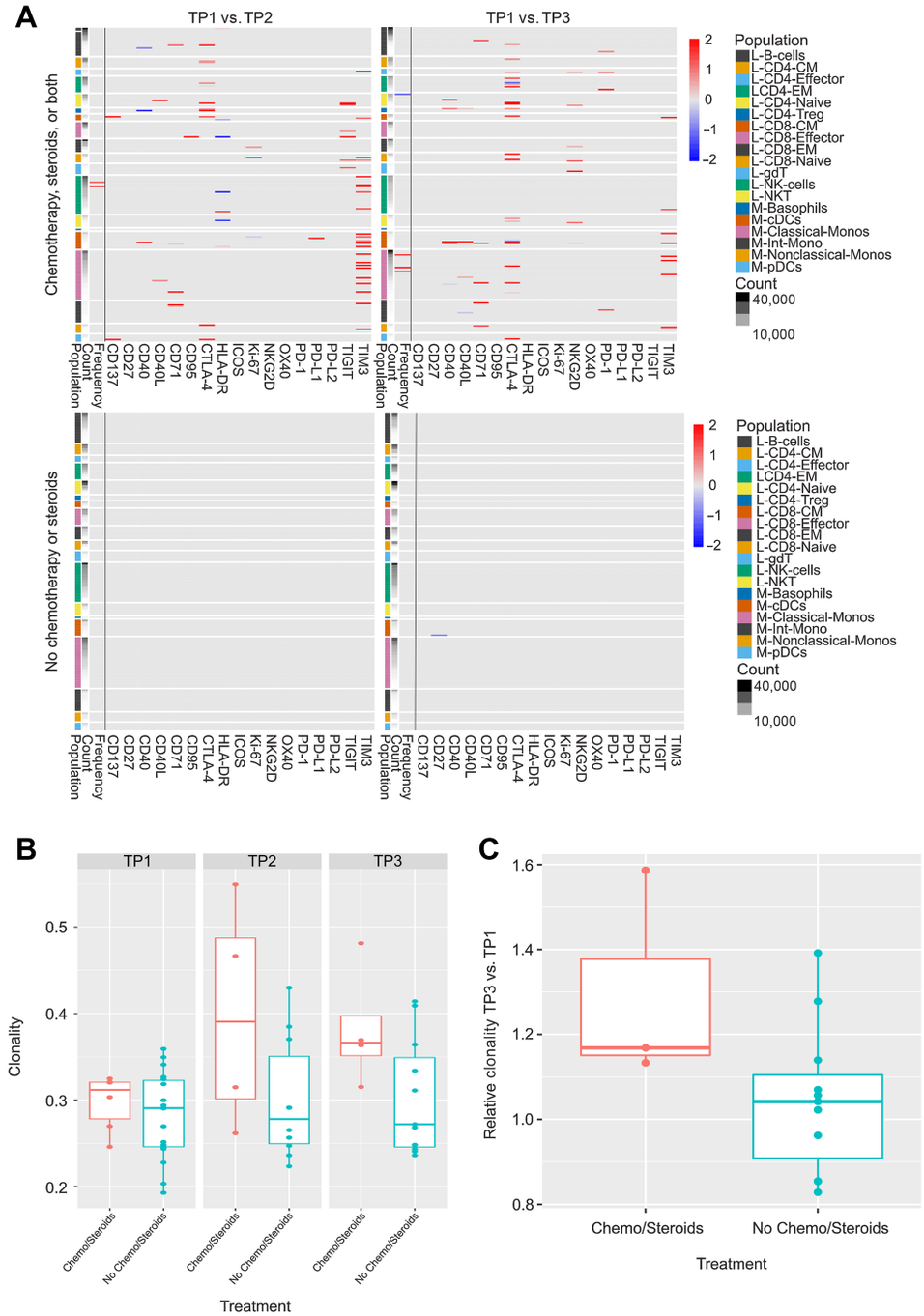

Figure 5.

Immune modulation in patients with or without chemotherapy (chemo)/steroids. **A,** Heat maps summarizing $\log_2$ fold changes from statistical analysis of functional markers CD137, CD27, CD40, CD40L, CD71, CD95, CTLA-4, HLA-DR, ICOS, Ki-67, NKG2D, OX40, PD-1, PD-L1, PD-L2, TIGIT, and TIM3 when comparing pretreatment time point TP1 (chemotherapy/steroids, $n = 5$; Denosumab only, $n = 11$) with TP2 (chemotherapy/steroids, $n = 6$; denosumab only, $n = 10$) and TP3 (chemotherapy/steroids, $n = 6$; denosumab only, $n = 8$) in patients received chemotherapy, steroids, or both (top) and patients who did not receive chemotherapy or steroids (bottom). Each box in the heat map represents a lymphocyte cluster that was labeled according to the nearest landmark node they connect to on the scaffold map and ordered by cell count abundance. The pseudocolor represents clusters that showed a significant difference ($q < 0.05$) in the $\log_2$ fold change, with red being significantly higher, while blue being significantly lower in group 2 of the two comparison groups. Heat maps were generated using statistical scaffold to analyze PBMC data obtained from CyTOF. TCR clonality (chemotherapy/steroids, $n = 6$; denosumab only, $n = 18$; **B**) and TCR relative clonality (chemotherapy/steroids, $n = 8$; denosumab only, $n = 18$; **C**) were calculated and compared between patients who did and did not receive chemotherapy or steroids across the time points using the Wilcoxon rank-sum test. In these box and whisker plots, the box covers the interquartile range, the horizontal line that splits the box is the median, and the whiskers capture the minimum and maximum.

analyzing TCR sequences from patients. Although not statistically significant, we observed a transient increase in clonality immediately after treatment, suggesting a narrowing of the repertoire. Yet, we did not notice any other significant changes or trends in clonality and TCR convergent frequency. RANKL upregulation has been shown in the contexts of T-cell response to tolerogenic signal (22) and peripheral $CD8^+$ T cells undergoing deletional tolerance (23). Thus, blocking the RANK–RANKL pathway with denosumab may play a role in the transient clonality increase we observed through tolerogenic mechanisms. We also investigated whether denosumab would lead to the generation of more thymic naïve T cells due to less stringent negative selection. We hypothesized that by disrupting the development of mTECs, denosumab would alter the self-tolerance in developing T cells (24). An increase in TRECs would suggest increased T-cell diversity (17), but we did not observe any significant differences in the amount of TRECs after denosumab treatment. The thymus involutes with age and is estimated to decline over time in thymic T-cell production with a half-life of about 15.7 years (25–27). Because the median age of our study patients is 67.5 years, the lack of observed change in TRECs could reflect the age-related decline in thymic function (28, 29). Perhaps if denosumab is used in a younger population, the outcomes of thymic emigrants may differ. Overall, these data suggest that denosumab minimally changes the diversity of both the peripheral T-cell population as well as recent thymic emigrants.

Stratifying our data by patients who received conventional cancer treatments, such as chemotherapy and corticosteroids, in combination with denosumab revealed greater immune modulation in patients who received these other therapies. In patients who received chemotherapy and/or steroids, we observed an increase in TIM3 expression across DC and monocyte populations and an increase in CTLA-4 in the T-cell compartment. Despite TIM3 facilitating DC antigen cross-presentation (30), other studies have shown that TIM3-expressing DCs inhibit activation of nucleic acid sensing Toll-like receptors (31) and weaken $CD8^+$ T-cell cytotoxicity indirectly (32). Thus, the implications of our observed increase in TIM3 expression are unclear. Patients that did not receive chemotherapy or steroids showed no changes in functional markers after receiving denosumab consistent with modest effects of denosumab on circulating immune cells. However, when we stratified patients at denosumab pretreatment TP1, the changes in activation markers were significantly more robust. Considering this, the changes observed in patients who received concomitant treatment could be due to pre-existing differences before denosumab treatment began. Further segregating the concurrent treatments also revealed greater immune modulation in patients who received chemotherapy or chemotherapy and steroids. Because steroids are commonly given together with chemotherapy as an antiemetic treatment, our interrogation of concurrent treatments was limited, as there was only 1 patient who received only chemotherapy. Furthermore, only 1 patient received only steroids prior to denosumab treatment, consequently limiting our pretreatment analysis to comparing chemotherapy or chemotherapy and steroids with no chemotherapy or steroids. Dividing the treatment groups also reduced our statistical power; 2 patients received only steroids at TP2 and 3 patients received only steroids at TP3. A more abundant sample size of patients across the various concomitant treatment groups is required to validate our observations. Our analysis of clonality in the T-cell repertoire revealed that clonality and relative clonality in patients who received chemotherapy, steroids, or both were not significantly different. This aligns with a previous finding that chemotherapy depletes T-cell subsets, but clonality does not significantly change (33).

The design of our study as a prospective, nonrandomized, biobanking protocol has limitations. Because of scope of the study, progression-free survival and overall survival were not captured to assess clinical outcomes. In addition, because patients received denosumab as standard of care, we were not able to obtain serial biopsies due to the attendant risks so analysis of changes in the tumor microenvironment could not be performed. Although we did not have a control cohort, we were still able to evaluate differences in the peripheral immune landscape longitudinally, because the first time point was obtained without denosumab. While our study provides insights into the immune modulation of patients with cancer receiving denosumab, this dataset is derived from a small cohort where only prostate and renal cell carcinoma are represented.

In summary, our data suggest that administering denosumab alone results in very modest changes with respect to immunomodulation, thymic T-cell generation, and peripheral T-cell repertoire. In contrast, administering denosumab with conventional cancer therapies, such as chemotherapy and corticosteroids, results in broad changes in phenotypic markers that include the induction of multiple immune checkpoints across multiple lymphoid- and myeloid-cell populations. Larger cohorts will be needed to separate the effects of steroids and chemotherapy, and to tease apart the mechanisms by which these treatments can sensitize these different immune populations to denosumab. Clinical data suggest that patients receiving corticosteroids either prior or during immune checkpoint inhibitor therapy differ in neither overall survival nor progression-free survival (34). Despite the limited effects of denosumab on the immune landscape, future studies should further explore the relationship of denosumab with concomitant cancer therapies including immune checkpoint inhibitors.

Authors' Disclosures

H. Chang reports grants from Amgen during the conduct of the study. M.L. Cheng reports personal fees from Pfizer, Mirati Therapeutics, Janssen, Boehringer Ingelheim, and AstraZeneca, and grants from Palleon Pharmaceuticals outside the submitted work. E.D. Chow is a founder of Survey Genomics. R.R. Aggarwal reports grants from Amgen and Janssen, grants and personal fees from AstraZeneca and Merck, and personal fees from Curio, Boxer Capital, PCCTC, Novartis, Lumanity, Targeted Oncology, Scitaris, and KeyQuest outside the submitted work. T.W. Friedlander reports grants and personal fees from Seagen, personal fees from Astellas, Aadi Biosciences, Merck, and Gilead, and grants from Roche Genentech outside the submitted work. E.J. Small reports personal fees and other support from Fortis, other support from Harpoon, and Teon, personal fees from J&J, Janssen, and Deciphera during the conduct of the study, and personal fees from J&J, Janssen, and Deciphera outside the submitted work. M. Anderson reports other support from Merck, Inc outside the submitted work. L. Fong reports grants and personal fees from Amgen during the conduct of the study, grants and personal fees from Abbvie, BMS, Dendreon, and Roche/Genentech, grants from, Bavarian Nordic, Janssen, Merck, and Nektar; nonfinancial support from Actym, Atreca, Bolt, Immunogenesis, Nutcracker, Scribe, and Senti; personal fees from AstraZeneca, Crescendo, Daiichi Sankyo, and Innovent, and personal fees and nonfinancial support from Bioatla, NGMBio, RAPT, and Sutro outside the submitted work. No disclosures were reported by the other authors.

Authors' Contributions

H. Chang: Data curation, formal analysis, writing–original draft, writing–review and editing. **J. Marquez:** Data curation, formal analysis. **B.K. Chen:** Visualization. **D.M. Kim:** Investigation. **M.L. Cheng:** Conceptualization. **E.V. Liu:** Formal analysis, visualization. **H. Yang:** Software, formal analysis, visualization. **L. Zhang:** Data curation, formal analysis. **M. Sinha:** Formal analysis, supervision. **A. Cheung:** Data curation, supervision. **S.S. Kwek:** Data curation, formal analysis, investigation. **E.D. Chow:** Software. **M. Bridge:** Data curation. **R.R. Aggarwal:** Data curation. **T.W. Friedlander:** Data curation. **E.J. Small:** Data curation. **M. Anderson:** Conceptualization. **L. Fong:** Conceptualization, formal analysis,

supervision, funding acquisition, writing–original draft, writing–review and editing.

Acknowledgments

The clinical trial was supported in part by Amgen. L. Fong was supported by a Prostate Cancer Foundation Challenge Grant and NCI R35CA253175.

Note

Supplementary data for this article are available at Cancer Immunology Research Online (http://cancerimmunolres.aacrjournals.org/).

Received February 27, 2023; revised September 21, 2023; accepted January 23, 2024; published first January 26, 2024.

References

1. Simonet WS, Lacey DL, Dunstan CR, Kelley M, Chang MS, Lüthy R, et al. Osteoprotegerin: a novel secreted protein involved in the regulation of bone density. Cell 1997;89:309–19.
2. Hanley DA, Adachi JD, Bell A, Brown V. Denosumab: mechanism of action and clinical outcomes. Int J Clin Pract 2012;66:1139–46.
3. Anderson DM, Maraskovsky E, Billingsley WL, Dougall WC, Tometsko ME, Roux ER, et al. A homologue of the TNF receptor and its ligand enhance T-cell growth and dendritic-cell function. Nature 1997;390:175–9.
4. Nopora A, Brocker T. Bcl-2 controls dendritic cell longevity *in vivo*. J Immunol 2002;169:3006–14.
5. Park D, Lapteva N, Seethammagari M, Slawin KM, Spencer DM. An essential role for Akt1 in dendritic cell function and tumor immunotherapy. Nat Biotechnol 2006;24:1581–90.
6. Totsuka T, Kanai T, Nemoto Y, Tomita T, Okamoto R, Tsuchiya K, et al. RANK-RANKL signaling pathway is critically involved in the function of CD4+CD25+ regulatory T cells in chronic colitis. J Immunol 2009;182:6079–87.
7. Akiyama T, Shimo Y, Yanai H, Qin J, Ohshima D, Maruyama Y, et al. The tumor necrosis factor family receptors RANK and CD40 cooperatively establish the thymic medullary microenvironment and self-tolerance [published correction appears in Immunity. 2013;39:796]. Immunity 2008;29:423–37.
8. Van Gassen S, Gaudilliere B, Angst MS, Saeys Y, Aghaeepour N. CytoNorm: a normalization algorithm for cytometry data. Cytometry A 2020;97:268–78.
9. Spitzer MH, Carmi Y, Reticker-Flynn NE, Kwek SS, Madhireddy D, Martins MM, et al. Systemic immunity is required for effective cancer immunotherapy. Cell 2017;168:487–502.
10. Levine JH, Simonds EF, Bendall SC, Davis KL, Amir el-AD, Tadmor MD, et al. Data-driven phenotypic dissection of AML reveals progenitor-like cells that correlate with prognosis. Cell 2015;162:184–97.
11. Picelli S, Björklund ÅK, Faridani OR, Sagasser S, Winberg G, Sandberg R. Smart-seq2 for sensitive full-length transcriptome profiling in single cells. Nat Methods 2013;10:1096–8.
12. Zhang L, Cham J, Paciorek A, Trager J, Sheikh N, Fong L. 3D: diversity, dynamics, differential testing - a proposed pipeline for analysis of next-generation sequencing T cell repertoire data. BMC Bioinformatics 2017;18:129.
13. Looney TJ, Topacio-Hall D, Lowman G, Conroy J, Morrison C, Oh D, et al. TCR convergence in individuals treated with immune checkpoint inhibition for cancer. Front Immunol 2020;10:2985.
14. Josien R, Wong BR, Li HL, Steinman RM, Choi Y. TRANCE, a TNF family member, is differentially expressed on T cell subsets and induces cytokine production in dendritic cells. J Immunol 1999;162:2562–8.
15. Rossi SW, Kim MY, Leibbrandt A, Parnell SM, Jenkinson WE, Glanville SH, et al. RANK signals from CD4(+)3(-) inducer cells regulate development of Aire-expressing epithelial cells in the thymic medulla. J Exp Med 2007;204:1267–72.
16. Khan IS, Mouchess ML, Zhu ML, Conley B, Fasano KJ, Hou Y, et al. Enhancement of an anti-tumor immune response by transient blockade of central T cell tolerance. J Exp Med 2014;211:761–8.
17. Bakhru P, Zhu ML, Wang HH, Hong LK, Khan I, Mouchess M, et al. Combination central tolerance and peripheral checkpoint blockade unleashes anti-melanoma immunity. JCI Insight 2017;2:e93265.
18. Ahern E, Harjunpää H, O'Donnell JS, Allen S, Dougall WC, Teng MWL, et al. RANKL blockade improves efficacy of PD1-PD-L1 blockade or dual PD1-PD-L1 and CTLA4 blockade in mouse models of cancer. Oncoimmunology 2018;7:e1431088.
19. Smyth MJ, Yagita H, McArthur GA. Combination anti-CTLA-4 and anti-RANKL in metastatic melanoma. J Clin Oncol 2016;34:e104–6.
20. Ahern E, Harjunpää H, Barkauskas D, Allen S, Takeda K, Yagita H, et al. Co-administration of RANKL and CTLA4 antibodies enhances lymphocyte-mediated antitumor immunity in mice. Clin Cancer Res 2017;23:5789–801.
21. Gómez-Aleza C, Nguyen B, Yoldi G, Ciscar M, Barranco A, Hernández-Jiménez E, et al. Inhibition of RANK signaling in breast cancer induces an anti-tumor immune response orchestrated by CD8+ T cells. Nat Commun 2020;11:6335.
22. Hochweller K, Anderton SM. Kinetics of costimulatory molecule expression by T cells and dendritic cells during the induction of tolerance versus immunity *in vivo*. Eur J Immunol 2005;35:1086–96.
23. Parish IA, Rao S, Smyth GK, Juelich T, Denyer GS, Davey GM, et al. The molecular signature of CD8+ T cells undergoing deletional tolerance. Blood 2009;113:4575–85.
24. Gardner JM, Devoss JJ, Friedman RS, Wong DJ, Tan YX, Zhou X, et al. Deletional tolerance mediated by extrathymic Aire-expressing cells. Science 2008;321:843–7.
25. Douek DC, McFarland RD, Keiser PH, Gage EA, Massey JM, Haynes BF, et al. Changes in thymic function with age and during the treatment of HIV infection. Nature 1998;396:690–5.
26. Murray JM, Kaufmann GR, Hodgkin PD, Lewin SR, Kelleher AD, Davenport MP, et al. Naive T cells are maintained by thymic output in early ages but by proliferation without phenotypic change after age twenty. Immunol Cell Biol 2003;81:487–95.
27. Sottini A, Serana F, Bertoli D, Chiarini M, Valotti M, Vaglio Tessitore M, et al. Simultaneous quantification of T-cell receptor excision circles (TRECs) and K-deleting recombination excision circles (KRECs) by real-time PCR. J Vis Exp 2014;(94):52184.
28. Palmer S, Albergante L, Blackburn CC, Newman TJ. Thymic involution and rising disease incidence with age. Proc Natl Acad Sci U S A 2018;115:1883–8.
29. Steffens CM, Al-Harthi L, Shott S, Yogev R, Landay A. Evaluation of thymopoiesis using T cell receptor excision circles (TRECs): differential correlation between adult and pediatric TRECs and naïve phenotypes. Clin Immunol 2000;97:95–101.
30. Nakayama M, Akiba H, Takeda K, Kojima Y, Hashiguchi M, Azuma M, et al. Tim-3 mediates phagocytosis of apoptotic cells and cross-presentation. Blood 2009;113:3821–30.
31. de Mingo Pulido Á, Gardner A, Hiebler S, Soliman H, Rugo HS, Krummel MF, et al. TIM-3 regulates CD103+ dendritic cell function and response to chemotherapy in breast cancer. Cancer Cell 2018;33:60–74.
32. Chiba S, Baghdadi M, Akiba H, Yoshiyama H, Kinoshita I, Dosaka-Akita H, et al. Tumor-infiltrating DCs suppress nucleic acid-mediated innate immune responses through interactions between the receptor TIM-3 and the alarmin HMGB1. Nat Immunol 2012;13:832–42.
33. Chun B, Pucilowska J, Chang S, Kim I, Nikitin B, Koguchi Y, et al. Changes in T-cell subsets and clonal repertoire during chemoimmunotherapy with pembrolizumab and paclitaxel or capecitabine for metastatic triple-negative breast cancer. J Immunother Cancer 2022;10:e004033.
34. Pinato DJ, Kaseb A, Wang Y, Saeed A, Szafron D, Jun T, et al. Impact of corticosteroid therapy on the outcomes of hepatocellular carcinoma treated with immune checkpoint inhibitor therapy. J Immunother Cancer 2020;8:e000726.